An End-to-End Polychromatic Fresnel Propagation Model of GPI

Christian Marois*[a,b], Bruce Macintosh[b], Rémi Soummer[c], Lisa Poyneer[b], Brian Bauman[b]
[a]Herzberg Institute of Astrophysics, 5071 West Saanich Road, Victoria, BC, Canada, V9E 2E7;
[b]Lawrence Livermore National Laboratory, 7000 East Ave., Livermore, CA USA 94550;
[c]American Museum of Natural History, Central Park West at 79th St., New York, NY USA 10024

ABSTRACT

The Gemini Planet Imager (GPI) is a future high-order coronagraphic adaptive optics system optimized for the search and analysis of Jupiter-like exoplanets around nearby young 10-1000Myr stars. In this paper, an on-axis Fresnel wavefront propagation model of GPI is presented. The main goal of this work is to confirm that the current GPI design will reach its 10^{-7} contrast requirement. The model, assembled using the PROPER IDL library, is used to properly simulate out-of-pupil-plane and finite size optics. A spectral data cube at GPI spectral resolution R=45 in H-band is obtained to estimate the GPI contrast as a function of wavelength. This cube is then used to evaluate the speckle suppression performance of the Simultaneous Spectral Differential Imaging (SSDI) technique. It is shown that GPI should achieve a photon noise limited 10^{-7} contrast when using a simple SSDI post-processing on an H=5 star and a 1h observing sequence. Finally, a long exposure data cube is obtained by combining the speckle contributions of an average atmosphere and GPI optics. That final long-exposure contrast as a function of wavelength can be used to estimate the GPI exoplanet characterization accuracy, and to evaluate, using Monte-Carlo simulations, the expected exoplanet survey performance.

Keywords: Imaging, Near-Infrared, Adaptive Optics, High-Contrast, Coronagraphy, Stars, Exoplanets, Image processing

1. INTRODUCTION

Directly detecting exoplanets around nearby stars using ground-based telescopes is a challenging endeavor. Atmospheric- and static-induced phase and amplitude wavefront errors are producing a complex interference pattern in the point-spread function (PSF) that can mask the faint signal from exoplanets.[1,2] To circumvent these problems, specialized planet imaging instruments like the Gemini Planet Imager (GPI) and VLT SPHERE combine a high-order adaptive optics (AO) system to precisely correct the wavefront with a coronagraph.[3,4] The goal is to remove the light of the star and reveal the light from planets.

Even with such highly accurate systems, hour-long integrations are not photon noise limited. Uncorrected/residual aberrations from the AO system and quasi-static errors from the telescope and instrument optics limit the achievable contrast. A detail model of the instrument optical prescription needs to be developed to adequately predict the achievable polychromatic contrast after hour-long integrations and to optimize, via surface polishing specifications and other AO/coronagraph parameters, exoplanet detections and their characterization.

Simple Fraunhofer analysis will usually significantly overpredict the performance of such systems. In this paper, a Fresnel propagation model of GPI is presented. The GPI instrument will be briefly described as well as its polychromatic contrast goal in Section 1. Section 2 presents the Fresnel model and the expected nominal polychromatic static contrast. Section 3 discusses several tolerance analyses. Long 1h-exposures are shown in Section 4 followed by conclusions in Section 5.

2. THE GEMINI PLANET IMAGER

The main Gemini Planet Imager (GPI) objective is to reach a broadband 10^{-7} contrast in the near-infrared to first detect and then characterize exoplanets and dust/gas circumstellar disks around nearby stars. The current GPI design consists of

Adaptive Optics Systems, edited by Norbert Hubin, Claire E. Max, Peter L. Wizinowich,
Proc. of SPIE Vol. 7015, 70151T, (2008)
0277-786X/08/$18 · doi: 10.1117/12.789899

an atmospheric dispersion corrector (ADC) to insure that the wavefronts at all wavelengths are aligned inside GPI, a high-order adaptive optics (AO) system to partially correct aberrations from the atmosphere, telescope, and GPI itself and produce a very flat wavefront, an apodized pupil Lyot coronagraph (APLC) to reject coherent light, an infrared calibration interferometer to estimate quasi-static aberrations at the science wavelength and an integral field spectrograph (IFS) with a polarizer module.[5-7] Even with such advanced design and precise (nanometer RMS) optics, at some angular separations and on bright targets, raw GPI images will not be limited by photon noise after 1-2h integrations. The contrast will be limited by residual atmospheric speckles and by uncorrected quasi-static speckles. Some kind of speckle suppression technique is needed to reach the photon noise limit and maximize GPI science capability.

Speckle suppression is the art of attenuating unwanted noise by using specific temporal (the Angular Differential Imaging technique ADI), spectral (the Simultaneous Spectral Differential Imaging), polarization and symmetry properties of an object that we are looking for that differ from the unwanted noise.[8-12] This paper is focusing solely on exoplanet detection and characterization. Since exoplanets are detected by their thermal emission in the near-infrared, GPI NIR polarization measurement capabilities are not analyzed here. For the rest of this paper, we will assumed that exoplanets are unpolarized point-like sources showing a cool spectrum that differs from their stellar primary.

For most simulations, the primary magnitude is selected to be 5 at H and 6 in the visible (I-band). The total observing sequence per object is 1h and the star is assumed to be typically 30 degrees from Zenith at transit (total field-of-view (FOV) rotation of 20 degrees in 1h). Two sources of speckle noise are considered here: (1) a random speckle noise coming from uncorrected atmospheric aberration and (2) a quasi-static speckle noise coming from the telescope and instruments. A basic ADI quasi-static speckle attenuation is assumed for most figures (calculated by assuming a gain equal to the square root of the total FOV rotation (in lambda/D) at each angular separation). SSDI speckle attenuation is treated separately.

The analysis presented in this paper is an important step forward compared to our previous analysis where all static speckle simulations were performed following the Talbot wavefront propagation approximation (valid only for small aberrations and collimated infinite wavefronts) while now a complete end-to-end Fresnel wavefront propagation tool is used instead. Although the new contrast curves are similar to the ones generated using the Talbot approximation, the Fresnel propagation properly account for edge effects/wavefront truncations and it can be used to simulate post-coronagraph optics up to the integral field spectrograph microlens array, dust particles and secondary spider vanes. In addition, the new gray APLC and an updated CAL residual error map are used to produce up-to-date GPI contrast predictions.

3. GPI FRESNEL PROPAGATION MODEL

SSDI attenuation performance is usually derived assuming the Fraunhofer approximation, thus assuming that all aberrations are in the pupil plane and that the PSF is simply the Fourier transform of the complex pupil (far-field approximation). Such simulations predict impressive speckle suppression performances; approaching 10,000 for the combination of three images at three wavelength.[10] It has been shown that in reality, out-of-pupil-plane aberration Fresnel propagation effects introduce phase-induced amplitude aberrations that evolve with wavelength.[13] In addition, other GPI components, like the coronagraph, can also produce additional chromaticity. These effects will change the ratio of symmetric (mostly unpinned) and anti-symmetric (pinned) speckles as a function of wavelength and prevent the SSDI technique to achieve its theoretical Fraunhofer speckle suppression goals. A complete understanding of GPI components and their response with wavelength is thus required to properly predict GPI SSDI attenuation performance.

3.1 The Fresnel Propagation

The Fresnel code used to simulate GPI optical prescription is called PROPER.[14] The IDL code first propagates a Gaussian beam to derive the best propagation technique between a far-field and an angular spectrum technique. The code can be called recursively to propagate through an optical system where the wavefront curvature is updated at each plane. At each propagation plane, phase and amplitude errors can be added to the wavefront. The ease of use and improve capabilities of such code is remarkable and will be demonstrated in the following sections.

3.2 GPI Optical Prescription

Simulations that are presented in this section are for all optics up to the IFS microlens array, i.e. up to the surface where the wavefront becomes incoherent (see Figure 3-1 for GPI optical layout).

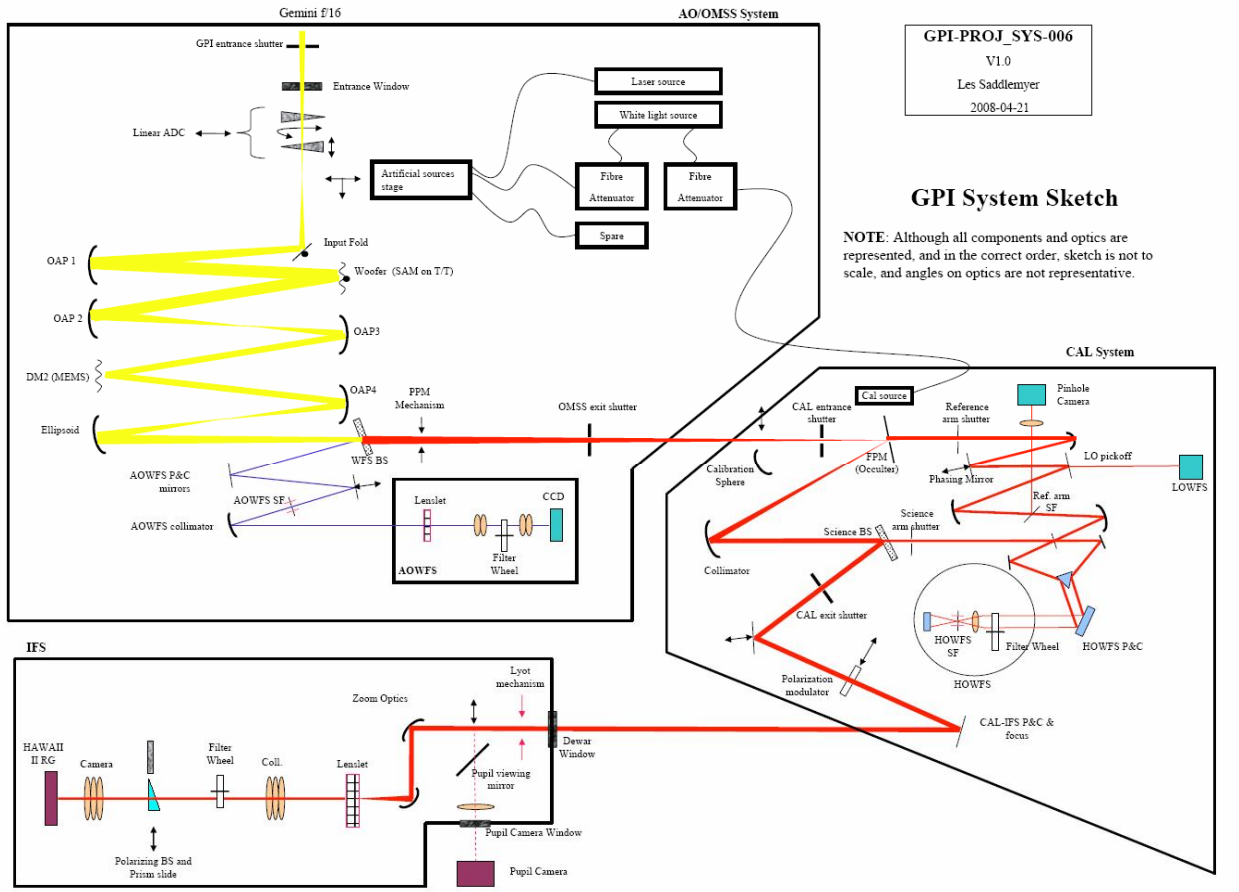

Figure 3-1 The GPI optical layout. Light from the telescope is coming from the above into GPI AO system. It is then transfered to the CAL interferometer and into the IFS.

An on-axis model of GPI is derived following GPI Zemax prescription (see Table 1). Typically, we have used 1 nm RMS phase aberration per surface for aberrations between 3-21 cycles and 5nm RMS for aberrations less than 3 cycles per pupil. A 0.1% RMS amplitude error (corresponding to 0.2% RMS intensity non-uniformities) is assumed for all surfaces. All aberration normalizations are performed inside the polishing area that will be quoted to vendors. The wavefront is also truncated at each surface to the specified optics diameter. All aberrations are generated using a -2.5 power-law that is flat for spatial periods bigger then the wavefront diameter.

Table 1 GPI on-axis prescription. The * sign means that 2 surfaces is assumed for that propagation plane. All aberrations are expressed in wavefront OPD.

Surface	Focal Length (m)	OD (m)	% dia. polish	Dist. to next surface (m)	0-3 cycles RMS WFE (nm)	3-21 cycles RMS WFE (nm)	Ampl. error (% RMS)
M1	14.40200	7.615	1.00	12.55573	5	45	0.23
M2	-2.07774	-	1.00	15.62260	5	21	0.23
M3	-	-	1.00	0.61100	5	10	0.23
Window*	-	0.05	0.38	0.04800	2.5	0.5	0.1
ADC01*	-	0.03	0.54	0.10700	7	1.4	0.14
ADC02*	-	0.03	0.50	0.45398	7	1.4	0.14
Folding flat	-	0.03	0.70	0.26998	2.5	0.5	0.1
OAP1	0.64438	0.05	0.88	0.66943	5	1	0.1
DM1	-	0.05	1.00	0.64438	-	-	0.1
OAP2	0.64438	0.05	0.86	0.93321	5	1	0.1
OAP3	0.28883	0.028	0.79	0.28883	5	1	0.1
DM2	-	0.05	1.00	0.28883	-	-	0.3
OAP4	0.28883	0.028	0.75	0.53845	5	1	0.1
Ellipse	0.19888	0.028	0.68	0.12000	5	1	0.1
WFS Beam-Splitter*	-	0.025	0.64	0.07888	7	1.4	0.14
PPM	-	0.025	0.52	0.77936	5	1	0.1
FPM	-	0.020	0.52	0.64642	5	1	0.1
Collimator	0.64642	0.04	0.85	0.24358	5	1	0.1
CAL Beam-Splitter*	-	0.04	0.73	0.22621	7	1.4	0.14
SF1	-	0.032	0.82	0.29236	2.5	0.5	0.1
SF2	-	0.032	0.63	0.42043	2.5	0.5	0.1
Lyot	0.64642	-	1.00	0.64642	-	-	-
Microlens	-	-	-	-	-	-	-

The prescription derived here differs slightly from the official GPI prescription since GPI is an off-axis design and the Fresnel propagation needs to be on-axis. All pupil-conjugated planes were checked by adding sine wave phase errors of different frequencies in the input pupil to confirm that all of them are perfectly in phase in all pupil-conjugated planes. Note that only the stop down pupil is propagated through the system, explaining the 7.615m diameter primary.

3.3 GPI Nominal Contrast

In the previous section, it was shown how GPI prescription was implemented with PROPER. More details on how the coronagraph, phase corrections and specific phase aberrations are simulated are now given. The following simulations have no atmospheric or dynamic phase errors, which would (over the short exposure times that can easily be simulated) completely swamp the static effects. We therefore evaluate dynamic and static effects independently and combine them later. Photon, sky and read noises as well as flat field errors are also neglected in this analysis and added separately into final science predictions. Different pupil/image size configurations are used depending on the resolution needed in the pupil plane and/or focal plane. For high-resolution pupil simulations, the entrance pupil has a 762 pixels diameter (~1cm/pixel) in a 2048x2048 pixels image. This pupil diameter is sufficient to properly simulate Gemini secondary support shadows as well as small-scale pupil phase errors and dust particles as discussed below. For simulations that do not require high pupil plane resolution, a 176 pixels diameter pupil is used in a 1024x1024 pixels image. For polychromatic long exposure PSFs that require thousand of PSF realizations, an 86-diameter pupil is used in a 512x512

pixels image. For all figures, a minimal ADI speckle attenuation gain through rotational averaging (not PSF subtraction) is assumed, but no SSDI post-processing is performed unless specified.

Coronagraphic PSFs are derived using a gray apodized Lyot coronagraph. The wavefront is propagated to the coronagaph conjugated pupil plane where it is multiplied with the pupil plane mask (PPM) and then propagated to the focal plane to derive the focal plane complex electric field. A focal plane mask (FPM) is then used to remove light from the central core of the PSF. The wavefront is then relayed by the collimator and by the two science folds to the Lyot plane. A slightly undersized pupil stop is multiplied to block coherent light that have been scattered outside the pupil and the wavefront is then finally propagated to the focal plane to derived the coronagraphic PSF intensity. If secondary spider vanes are included in the simulation, the Lyot stop also has a 2% oversized (2% of the pupil diameter) spider mask. The APLC coronagraph operates by carefully matching the pupil-plane response of its FPM to the PPM. Since the FPM's effective size in units of λ/D is obviously a function of wavelength, this tuning operates less well as λ changes.

Static phase aberrations are assumed to be detected at the science average wavelength by the GPI infrared calibration interferometer (CAL) and to be fully corrected through feedback to the deformable mirror. Since GPI can only correct phase aberration achromatically in the pupil plane and since the CAL system will measure aberrations up to the FPM, the phase aberration at the average science bandpass is first propagated up to the FPM and then back to a pupil plane to compute a reference phase screen that is applied to correct the aberrated wavefront at all wavelengths of the science bandpass. Since the phase aberration screen is evolving as a function of wavelength due to the chromatic phase and amplitude mixing (the Talbot effect), some phase aberrations will leak through the system at wavelengths that differ from the science average wavelength. Phase correction within our controlled spatial frequency range is assumed to be perfect at the science average wavelength, i.e. at that wavelength, all phase aberrations that have less than 21 cycles per pupil is fixed to zero. Reference non-coronagraphic aberrated PSF intensities (these are used to calibrate the contrast) are simply obtained by propagating the wavefront through the system without the FPM. Finally, a small systematic residual in the CAL measurements is re-injected into the wavefront.

The following subsections show GPI predicted contrast for the nominal surface aberrations and with some CAL residuals and additional effects (dust particles and spider vanes) that can now be simulations with the Fresnel propagation. The contrast is measured by first obtaining the noise RMS inside a 1 FWHM annulus of increasing diameter and by then dividing this value by the unocculted PSF peak intensity.

GPI contrast using only the prescription described in Section 3.2 (no M3) is now calculated in H-band for 1.48, 1.57 and 1.78 microns, the edges and middle of H-band (see Figure 3-2). The coronagraph is optimized at 1.65 microns and the CAL system perfectly corrects the phase at that same wavelength.

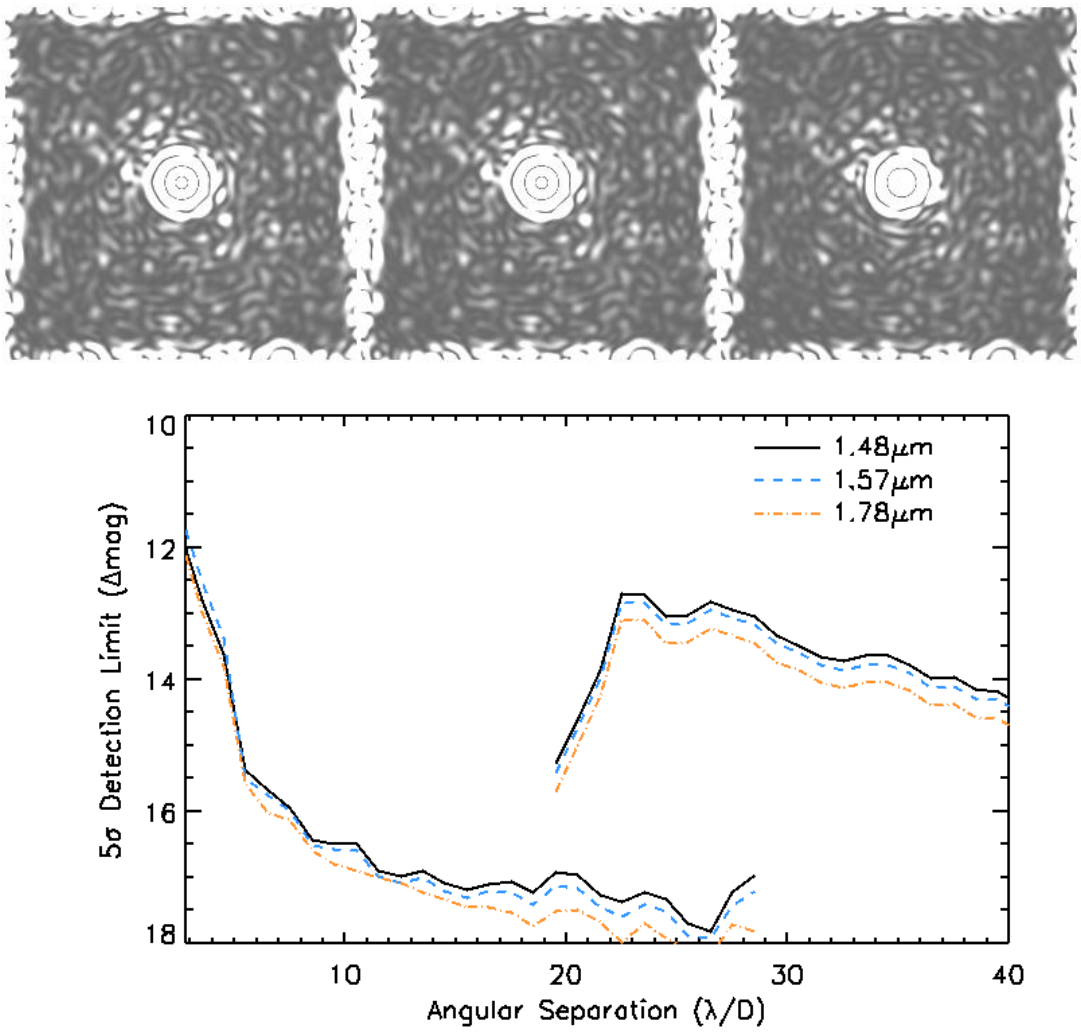

Figure 3-2 The GPI static PSF images/contrast at three wavelengths for the nominal surface aberrations. Upper three panels show the simulated coronagraphic PSFs at (from left to right) 1.48, 1.57 and 1.78 microns with the same intensity range and linear gray scale. The bottom panel shows a 5 sigma contrast detection limit in-and-out of the dark hole at 1.48, 1.57 and 1.78 microns. A 1h ADI speckle attenuation gain is assumed for the bottom panel.

The contrast obtained using the Fresnel propagation is very similar to the one obtained using the Talbot propagation. The main difference from previously presented results are coming from the new gray APLC that is much more achromatic while delivering a noisier PSF for separations less than ~8 lambda/D. Different combinations of PPM-FPM will be mounted in the instrument to offer different sets of inner working angles and chromaticity to minimize the telescope time required for detection & characterization of specific science cases.

4. TOLERANCE ANALYSIS

4.1 Observations with/without M3

The Gemini telescope supports Cassegrain instruments in either an up-looking or side-looking orientation, with the latter using a fold mirror (M3). Observations with and without M3 are now analyzed (see Figure 4-1). M3 aberrations are

simulated with a 10nm RMS WFE between 3 and 21 cycles per pupil and 0.23% amplitude. As with other surfaces, a -2.5 power-law is used to generate both phase and amplitude aberration screens.

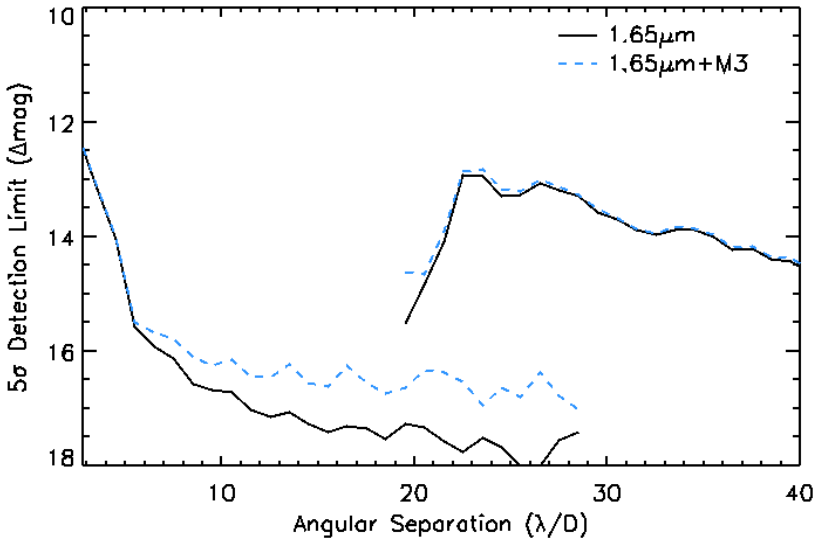

Figure 4-1 The GPI contrast with the nominal surface aberrations (solid black line) and with M3 (blue dashed line). A 1h ADI contrast gain is assumed.

Observation with M3 is not advisable since it lowers the contrast inside the dark hole by as much as a magnitude. This occurs since simulated mirror is both of significantly lower quality than GPI internal mirrors and (unlike the telescope primary and secondary) moderately close to focus, so Talbot-induced aberrations are stronger for it than any other optic in the system.

4.2 CAL Residuals

CAL interferometer residual aberrations are here assumed to be a combination of a low and mid-frequency phase aberrations (a nominal value of 5nm RMS of 0-3 cycles/pupil phase aberration and 1nm RMS of 3-21 cycles/pupil aberration). For the simulations presented here, this error is assumed to be static for an hour-long integration. The CAL residuals would thus act as a noise floor achievable by GPI. Figure 4-2 shows the contrast for a combination of 5/1nm RMS of low and mid-spatial frequencies phase aberration as well as a combination of 5/2 nm RMS and 5/5nm RMS.

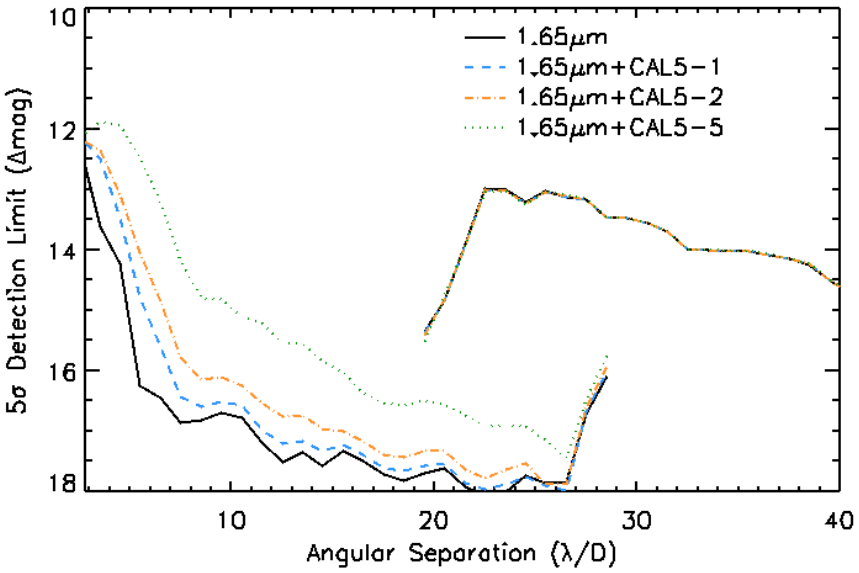

Figure 4-2 The GPI 1.65 microns contrast for the nominal surface aberrations (black line) and with an addition phase error from the CAL system. The blue dashed line if for a 5/1 nm RMS of low/mid spatial frequencies CAL phase aberrations, while the orange dot-dashed and green dotted lines are for a 5/2 and 5/5 nm RMS of CAL residuals. A 1h ADI contrast gain is assumed in this figure.

The CAL residuals lower the contrast for separations less than ~8 lambda/D due to the 5 nm low-frequency residuals. As the mid-frequencies are increased, contrast is reduced at all angular separations inside the dark hole. The current goal is to achieve a 5/1 nm RMS of residuals.

4.3 Secondary Spider Vanes

Secondary spider vane shadows are now included in the simulation. Due to the problem of requiring a good pupil plane sampling to include the spider vanes, a good image plane sampling to have a smooth and round FPM and images less than 2Kx2K to propagate the wavefront in a short amount of time, a 1 pixel width spider is simulated with the 762 pixel diameter pupil in a 2Kx2K image, thus corresponding to 1cm width spider vanes. The spider vanes affect the contrast in several ways. First, the propagation of the sharp spider shadows through the systems and the truncation of the wavefront (especially at the FPM) widens the spider flux profile at the Lyot plane. For that reason and the fact that an alignment margin needs to be considered due to a potential pupil misalignment from an instrument flexure, the spider mask needs to be oversized. Secondly, the Lyot plane spider mask has the detrimental effect of bringing flux from outside the dark hole, lowering the achievable contrast inside of it. This fact can be easily understood by remembering that the multiplication of two functions is equal to the convolution of the Fourier transform of these two functions. The Fourier transform of the spider mask is a narrow "X" function with a SINC intensity profile. Since the spider mask will be oversized by ~2% of the pupil diameter, the FWHM of the SINC function is ~50 lambda/D, or approximately equal to the dark hole diameter (42x42 lambda/D). The convolution of the coronagraphic PSF by this function will scatter some amount of flux from outside the dark hole and the speckle noise inside of it will be higher. Figure 4-3 shows the contrast for a spider mask oversizing of 1, 2 and 4% of the pupil diameter.

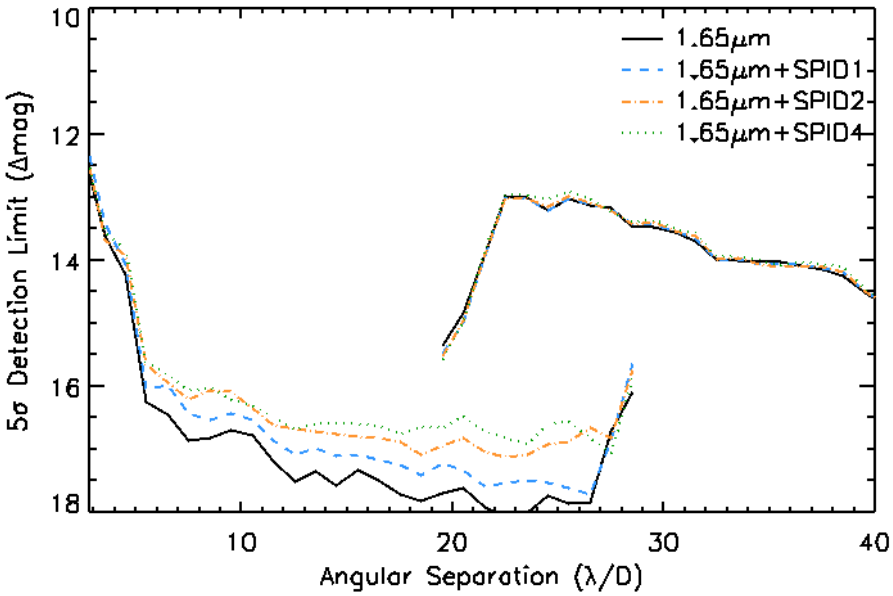

Figure 4-3 The GPI contrast using the nominal optical surface aberrations (black line) and including the spider vane shadows. The dashed blue line shows the contrast with a 1% Lyot spider mask oversizing (1% of the pupil diameter), while the orange dot-dashed and green dotted lines show respectively the contrast for a 2% and 4% Lyot spider mask oversizing. A 1h ADI contrast gain is assumed in this figure.

The spider vane shadows and Lyot spider mask do have an impact of the achievable contrast. A 4% oversizing of the Lyot mask lower the contrast by ~1-1.5 magnitudes between 10-27 lambda/D.

4.4 Dust Particles

Dust particles are simulated assuming a US standard cleanliness level of 300 inside the instrument. Since the instrument window will be exposed to dusty air, it is simulated with a cleanliness of 1000 on the exterior and 300 inside of the instrument. No dust is simulated on the primary, the secondary or M3 due to the large wavefront size ratio between those mirrors and typical dust particles. The dust surface density and particle size are simulated following known distributions of clean environment (see **Table 2**)

Table 2 Dust particle distributions for US STD cleanliness 300 and 1000.

	Cleanliness 300					Cleanliness 1000				
Particle size (microns)	25	50	100	250	300	100	250	500	750	1,000
Particles/0.1m^2	8,050	1,100	103	2.48	1.08	46,100	1,100	42.1	5.18	1.08

Dust particles are assumed to be round. Particles that are smaller than 1 pixel diameter are simulated with a single pixel circular particle but with a partial transmission set by the relative area of a pixel compare to the one of the dust particle. For FPM dust particles, the dust is convolved by a 2 pixels FWHM Gaussian to allow for accurate spatial scaling of the dust distribution on that plane as a function of wavelength (simulations are done with a fixed pupil and image sizes). Internal transmissive optics have twice the surface densities to account for the 2 surfaces. **Figure 4-4** shows the contrast with various cleanliness levels on the instrument window.

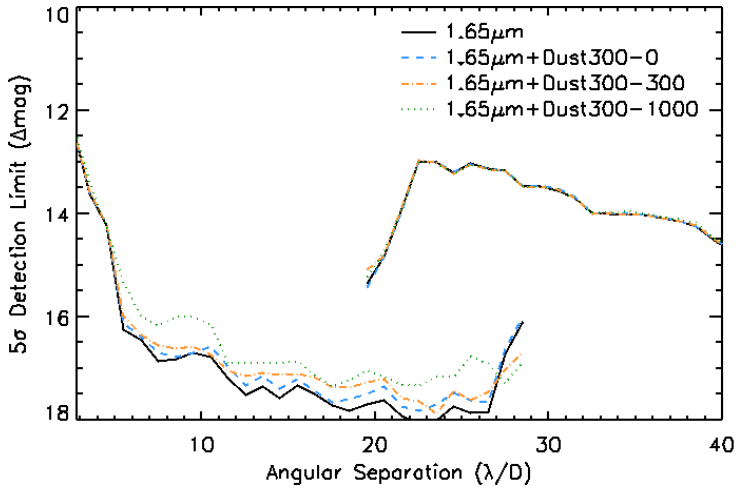

Figure 4-4 The GPI contrast using the nominal surface aberrations (solid black line) and including a distribution of dust particles on each optical surfaces. The blue dashed line shows the contrast for a cleanliness of 300 inside the instrument and no dust on the window exterior, while the orange dot-dashed and green dotted lines show respectively the contrast for a cleanliness of 300 inside the instrument and a cleanliness of 300 and 1000 on the window external surface. A 1h ADI contrast gain is assumed.

A cleanliness of 300 for the instrument interior is adequate for GPI predicted nominal contrast. The window surface that is exposed to dusty air could be problematic if large particles accumulate on it. A cleanliness of 1000 does show a ~1 magnitude decrease of contrast. The GPI window will be designed to be cleanable and incorporate an air knife that will be periodically used to wash away dust particles to obtain an average cleanliness level of.

5. GPI POLYCHROMATIC SIMULATIONS

Using the simulations that are described in Section 3, polychromatic PSFs are generated at H-band to predict GPI unprocessed PSF contrast and SSDI performances. All effects that are discussed in Section 4 (except M3) are included using their nominal values. The FPM is spatially adjusted to have a fixed size (in meter) at all wavelength. The dust particle distribution at the FPM plane is also spatially scale to assure that the dust is at the same physical position after spatially scaling the PSF to have an equal sampling per pixel at all wavelengths. **Figure 5-1** show the propagated wavefront up to the PPM and at the Lyot plane at 1.65 microns.

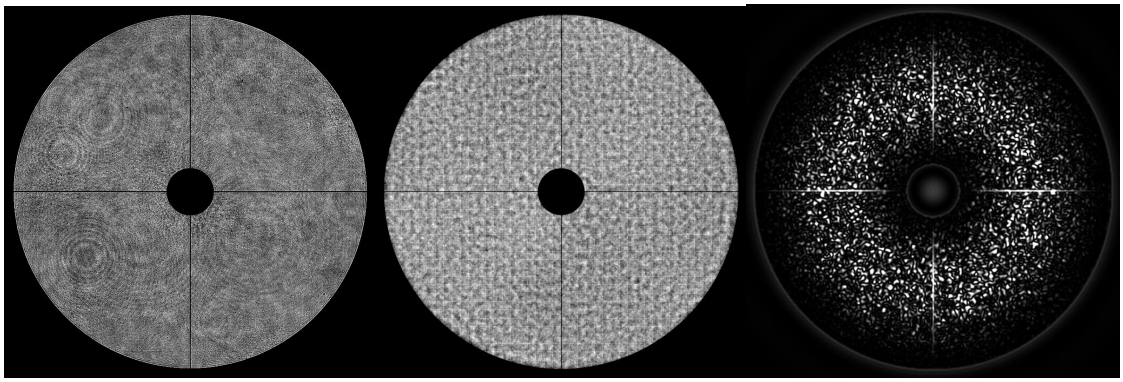

Figure 5-1 The GPI static PSF wavefront intensity at the PPM plane (before multiplying by the coronagraph PPM) at 1.65 microns (wavefront intensity is found in the left panel while the corresponding phase error is found

in the middle panel). Dust particles in-and-out of focus are easily visible on the wavefront as well as the secondary spider vanes. The wavefront intensity at the Lyot mask is shown in the right panel.

Dust particles in-and-out of focus are easily visible on the wavefront at the PPM plane as well as the tweeter print-though phase aberration (see **Figure 5-1**). Analysis of the Lyot plane image shows that the spider vane shadows have a ~4 pixels FWHM, thus four times larger than their original width. This smoothing effect is the result of the focal plane FOV trimming that convolved the pupil by a PSF having here a ~4 pixels FWHM. Figure 5-2 shows the raw image/contrast at 1.48, 1.57 and 1.78 microns respectively, i.e. the two edges of the H-band (1.48 and 1.78 microns) and the average bandpass where planets are expected to be bright (1.57 microns). The coronagraph optimal wavelength is chosen here to be 1.65 microns, matched near the bright part of the methane absorption features. The CAL system is perfectly correcting the phase at 1.65 microns.

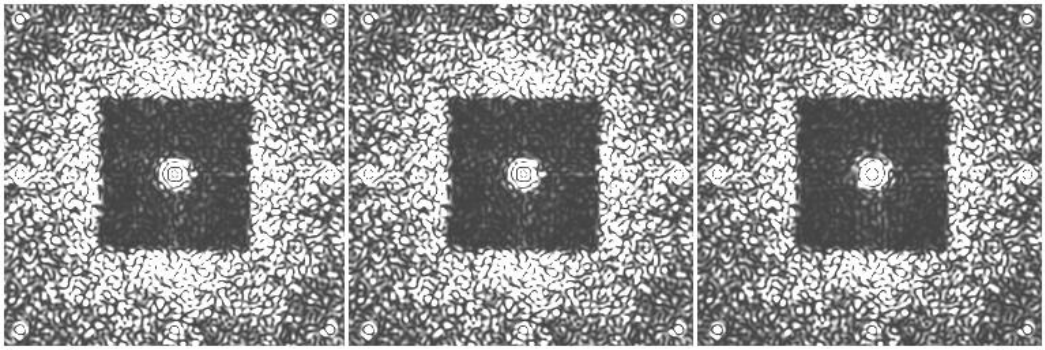

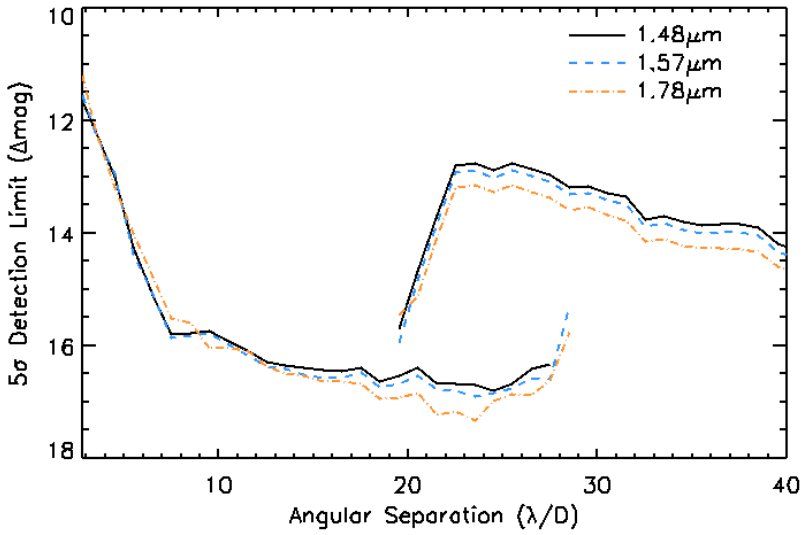

Figure 5-2 GPI static PSF raw images/contrast. Upper three panels show the simulated coronagraphic PSF at (from left to right) 1.48, 1.57 and 1.78 microns with the same intensity range and linear gray scale. The bottom left panel shows a 5 sigma contrast detection limit in-and-out of the dark hole at 1.48, 1.57 and 1.78 microns. A 1h ADI speckle attenuation gain is assumed for the bottom panel.

The new gray APLC coronagraph is much more achromatic than the previous design, offering simultaneous good detection and characterization performances. Its only current drawback is a reduced contrast <8 lambda/D. Figure 5-3 shoes the expected contrast gain using the SSDI technique.

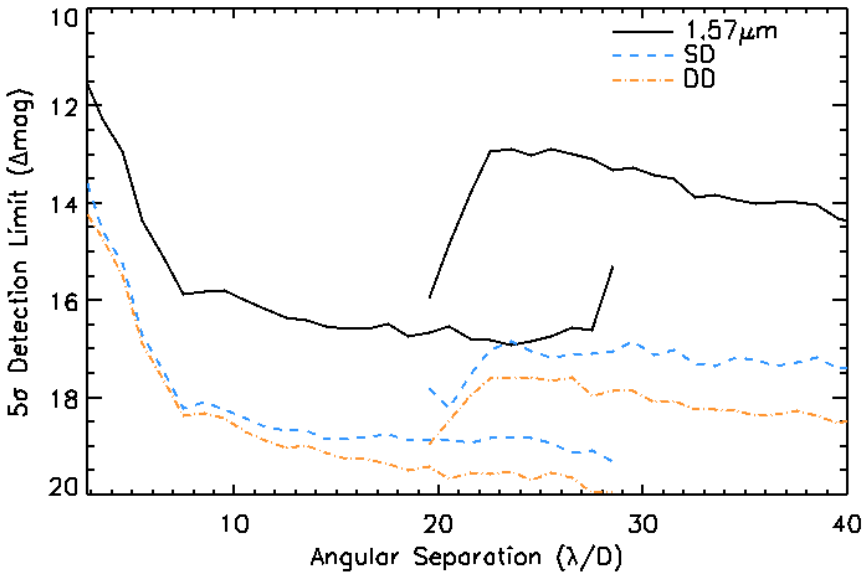

Figure 5-3 The raw GPI contrast (solid line) at 1.65 microns and the contrast after a SD ($I_{1.57} - k_{SD}\ I_{1.515}$, blue dashed line) and DD ($[(I_{1.57} - k_{SD1}\ I_{1.515}) - k_{DD}\ (I_{1.57} - k_{SD2}\ I_{1.625})]/k_N$, orange dot-dashed line). A 1h ADI contrast gain is assumed.

Typically, a SD improves the contrast by ~2 magnitudes and a DD further improves up to one magnitude.

6. SIMULATED 1H-LONG INTEGRATIONS

6.1 1-hour Long Reconstructed PSFs

A sequence of 2s atmosphere-only exposures are compared to static PSFs derived from the Fresnel-propagated static aberrations to evaluate the relative importance of atmospheric and static speckle noises after an hour-long integration. The atmospheric speckle noise is estimated by differencing the 2s AO PSFs and by normalizing the residual speckle noise by the square root of the integration time. The photon noise is estimated from the AO PSF intensity profile. Total flux of the PSF (obtained by obtaining a long-exposure PSF without the FPM) is normalized to the one expected from an hour-long integration on a magnitude H=5 star. A 15% throughput is assumed with a ~3% bandpass. Figure 6-1 shows the atmospheric speckle noise compare to the static speckle noise for an hour-long integration.

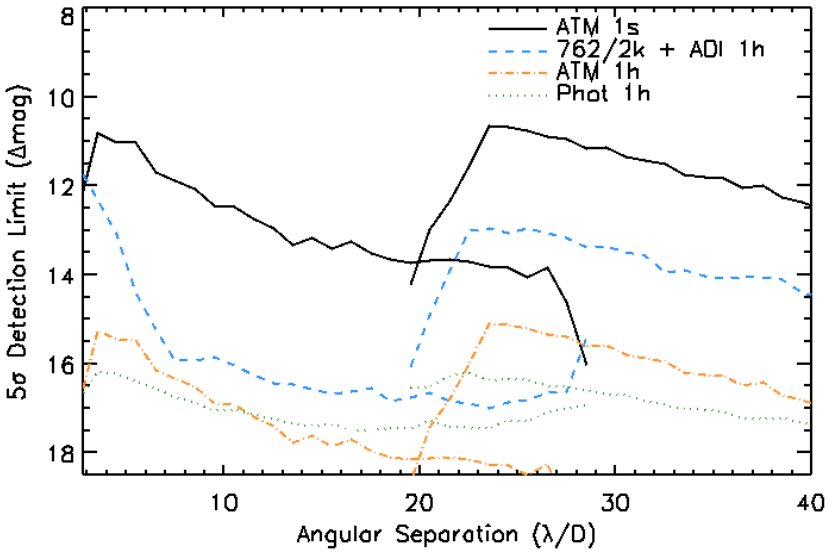

Figure 6-1 The predicted GPI contrast for an hour long integration. The black solid line shows the atmospheric speckle noise after 1s integration while the orange dot-dashed line shows the same noise after an hour integration. The blue dashed line represents the static speckle noise from the 762 pixels diameter pupil (2Kx2K image) simulation (all aberrations/effects with nominal values; no M3). The green dotted line shows the expected photon noise from a magnitude 5 star at H-band. A 1h ADI gain is assumed for the static speckle noise.

It is expected that after an hour-long integration, GPI will be static speckle noise limited at all angular separations. The photon noise can be achieved if the PSF is stable enough that ADI image processing can be used for PSF subtraction or if an SSDI-type image processing is applied. Figure 6-2 shows the expect SSDI gain (a DD obtained by combining the 1.515, 1.57 and 1.625 microns images) for both the atmosphere and static speckles.

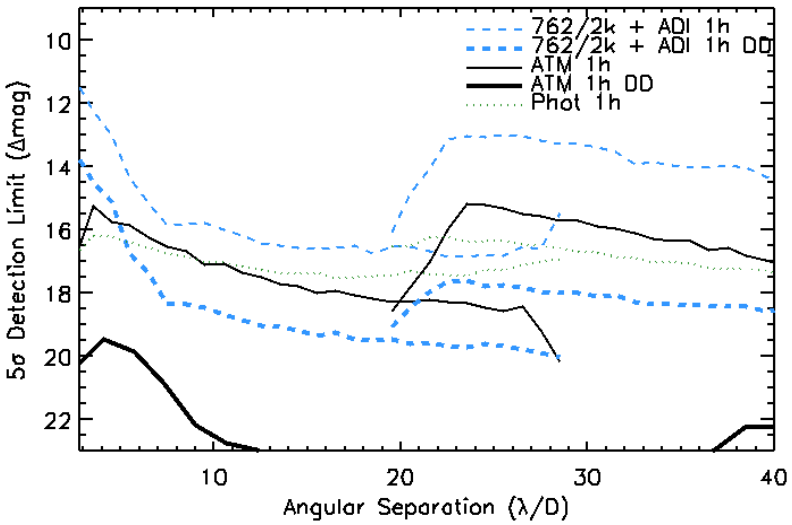

Figure 6-2 The GPI 1h long exposure predicted SSDI contrast. The thin blue dashed line shows the static 762 pixels diameter (2kx2k image) speckle noise simulation while the thick blue dashed line shows the resulting SSDI DD of that noise. The thin black line shows the 1h average speckle noise while the thick black line shows its DD. The green dotted line represents the 1h photon noise limit for an H-band 5 magnitude star. A 1h ADI gain is assumed for the static speckle noise.

The SSDI processing is sufficient to reach the expected photon noise limit at all angular separations for atmospheric speckles. Accurate atmospheric speckle noise attenuation was expected since the aberrations producing them are conjugated to the pupil. SSDI processing of static speckles is less effective due to Fresnel propagation effects, but still reach the photon noise limit for all separations greater than 5 lambda/D.

6.2 1-hour Long Simulated PSFs

Generating long-exposure PSFs is valuable for several reasons. First, static and atmospheric aberrations can be properly combined to confirm that no interference term between these two aberration sources prevent GPI to reach its contrast goal. It also allows the simulation of dust particles located on the FPM. SSDI speckle noise attenuation performances can be estimated with more realistic PSFs. The treatment of photon noise is also much simpler than reconstructed PSF since it is only a pixel-to-pixel Poisson noise addition after a simple PSF flux normalization. It is currently impossible to run the complete GPI AO simulator into the Fresnel propagation code to produce long-exposure PSFs (it would require significant CPU resources), an hybrid solution is thus used instead.

A 1s sequence of corrected atmospheric phase screens (running at 1.5 KHz) for an I=6 (H=5) star were generated using a full physical-optics AO simulator for the GPI optimal gain controller architecture. This sequence is used to simulate hour-long exposures using both the static and atmospheric noises. An average power-law of the residual atmosphere phase screens is first obtained by averaging the individual Fourier transform of each phase screen. A low-order polynomial is then fitted line-per-line and column-per-column to produce a smooth power-law in-and-out of the dark hole. Such fit is necessary to produce a smooth PSF atmospheric halo with increasing integration time. Figure 6-3 shows the average power-law compare to the low-order polynomial fit.

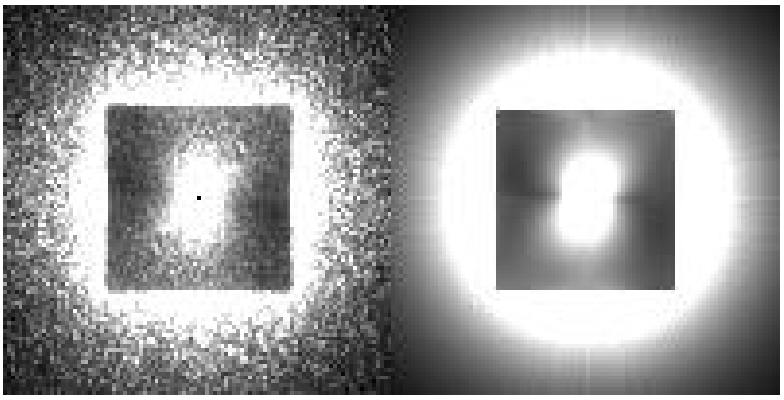

Figure 6-3 An atmospheric residual average power-law (left) from a 1s exposure I=6 star and its fitted profile (right) using low-order polynomials.

Uncorrelated atmospheric residual phase screens are then generated by taking the Fourier transform of the fitted power-law with a random phase shift for all spatial frequencies. Static aberrations are then added to each atmospheric residual screen by adding the Fresnel propagated static phase aberration (up to the PPM plane (no M3); post PPM optics are neglected – a good approximation since most of the light is removed by the FPM) and by multiplying by the static amplitude errors. The focal plane PSF is obtained by applying the APLC coronagraph. Each simulated phase screen is approximated constant for ~0.3s, i.e. the atmospheric approximate average speckle lifetime.[15] An hour-long exposure thus requires ~12,000 independent atmospheric speckle noise realizations (here rounded at 10,000, equivalent to choosing a pessimistic speckle life time of 0.36s).

Long-exposure polychromatic PSFs are now calculated. For these simulations, the atmosphere residuals, the static aberrations up to the PPM and dust particles on the FPM are included. Due to the large amount of FFTs required for generating the spectral data cube, small 86 pixels diameter pupils are used in 512x512 pixel images. Some effects like the tweeter print-through and scallop aberrations as well as the secondary spider vanes are neglected (although the spider vanes are not included in the simulation, the oversize Lyot mask does include the spider vane mask). The Fresnel

propagation is first calculated to derive a complex pupil for each wavelength. Off-axis ghost images of the primary are produced by including an amplitude sine wave aberration on the PPM.[16,17] Such copies of the primary are important for accurate photometry and astrometry of exoplanets. The atmosphere aberration is then added and 10,000 atmospheric speckle noise realizations are computed at each wavelength. The same speckle noise realization is used for each wavelength, thus simulating simultaneous observations required to estimate SSDI speckle noise attenuation performances. A total of 15 wavelengths are simulated at H-band. The 1h integrated PSF at 1.48, 1.57 and 1.78 microns are shown in Figure 6-4.

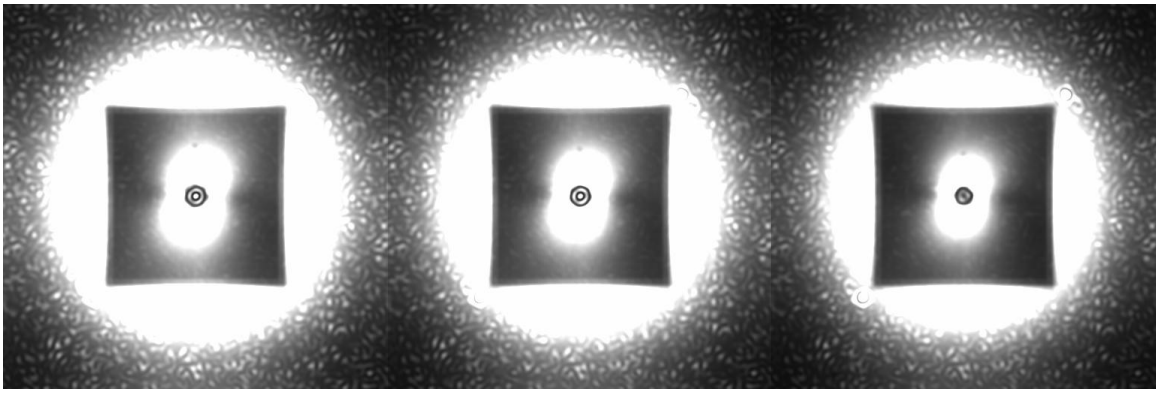

Figure 6-4 The GPI 1h long-exposure PSFs at 1.48 microns (left panel), 1.57 microns (middle panel) and 1.78 microns (right panel).

SSDI speckle noise attenuation performances are estimated by including the photon noise (magnitude 5 stars with 15% throughput). The spectral resolution is 64 since 15 wavelengths are simulated inside the H-band. Images are then binned together to produce 3 PSFs at 1.515, 1.57 and 1.625 microns having a ~3% bandpass. A Δmag = 11.3 background star as well as 2 planets (4 and 1 M_{Jup}, spectrum from the Baraffe et al. 2003 COND0 models) are also added in the image to show how their flux is retained during the SSDI process.[18] The more massive planet has a contrast of 12.1 magnitudes in its brightest spectral channel while the less massive planet has a contrast of 15 magnitudes also in its brightest spectral channel. The star spectral type is G2V located at 20pc and the 2 planets semi-major axes are 11 AU and 6 AU. The achievable SSDI speckle attenuation images and corresponding contrast (contrast curves were calculated without the background objects and 2 planets) are shown in Figure 6-5 after a convolution of a lambda/D diameter aperture.

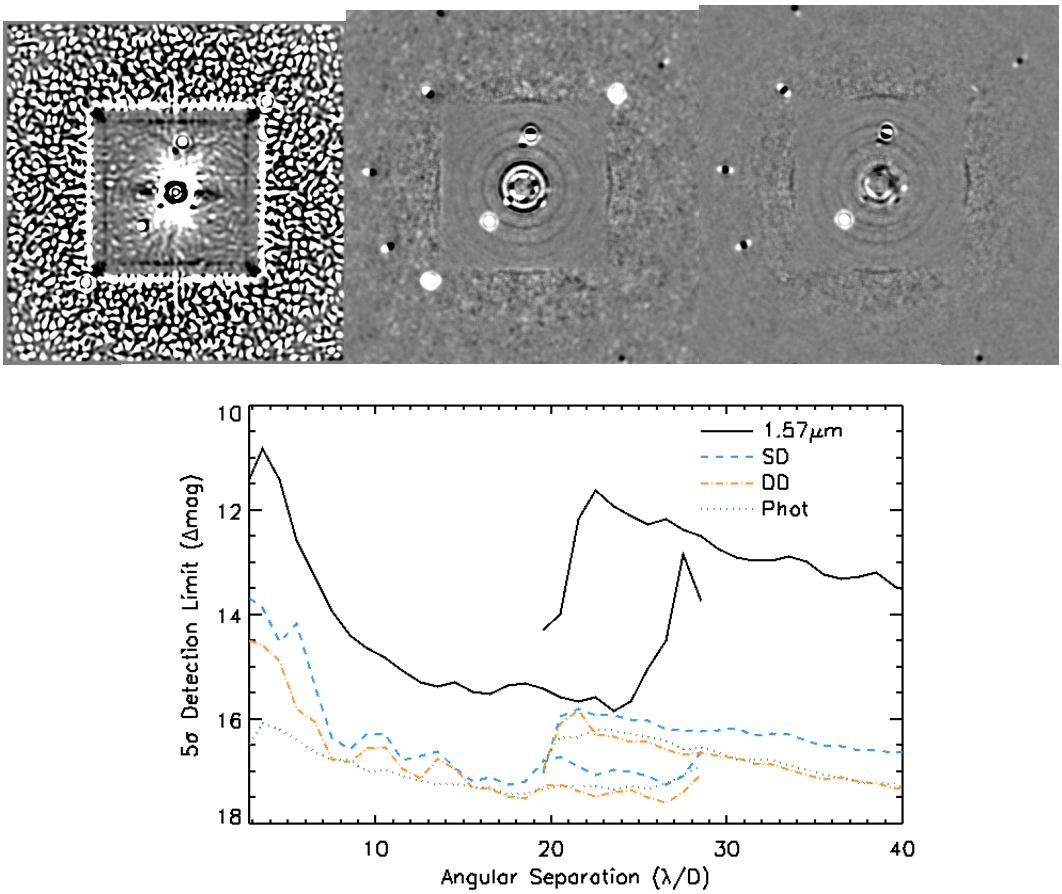

Figure 6-5 The GPI 1h long SSDI simulated images (above three panels). The Fresnel propagated static aberrations up to the PPM are included as well as dust particles on the FPM. The upper left panel shows the simulated PSF at 1.57 microns after applying an unsharp mask to remove the smooth halo. The upper middle panel shows the SD image while the upper right panel shows the DD. The photon noise is included for an H=5 star. All PSFs have been convolved by a 1 lambda/D diameter circular aperture. Images are shown with a linear gray scale between -5E-7 and 5E-7 of the PSF peak (after convolution by the aperture). The object North of the star is the background object while the 2 objects South and West of the star are the 2 planets. The one located Southeast of the star is a 4 Mjup/580K planet while the one West of the star is a 1 Mjup/330K planet. The 2 bright symmetric PSFs that are located Northwest and Southeast of the star are off-axis ghost images of the primary that are used for photometric/astrometric calibration of exoplanets. The bottom panel is the corresponding contrast curves. The solid black line shows the contrast at 1.57 microns after removing the smooth halo with an unsharp mask. The blue dashed line and the orange dot-dashed line show the contrast after SD and DD SSDI processing. The green dotted line shows the photon noise limit. Note that no ADI gain was applied here since atmospheric speckles (that do not get fainter with ADI) are mixed with static aberrations.

From this analysis, it is expected that GPI will reach with simple SSDI processing the photon noise limit for an H-band = 5 magnitude star for separations greater than ~8 lambda/D. Both the SD and DD can significantly reduce the speckle noise inside and outside the dark hole. The speckle noise attenuation gain outside the dark hole is explainable by the fact that most aberrations in that area originates from the telescope mirrors, thus very well pupil conjugated/behave smoothly with wavelength. Dust particles on the FPM are detectable in the SD and DD images. It is expected that those will be removed by a flat field image normalization. They were left here to illustrate their minimal impact on image quality.

Both the SD and DD clearly show the background object and the 4 M_{Jup} planet. The close-in 1Mjup/330K planet is only detected in the DD image.

7. CONCLUSIONS

An end-to-end Fresnel propagation model of GPI was used to demonstrate that GPI, with its current design, achieves a 10^{-7} photon noise limited contrast at a few lambda/D. A speckle attenuation technique (ADI and/or SSDI) is required to achieve photon noise limited detections. The same software has been used to but constraints on various instrument parameters (CAL residuals, observations with/without M3, dust particles and secondary spider vanes/Lyot mask). CAL residuals need to be less than 1 nm RMS for mid-spatial frequencies. Data acquisition without M3 is advisable since it could deteriorate the contrast inside the dark hole by as much as a magnitude. Dust particles are not a concerned except on the entrance window; periodic cleaning of it is required. The secondary spider vanes are properly block by the Lyot mask, but the required over-sizing of it due to instrument flexure and pupil misalignments degrade the contrast inside the dark hole. The spider vane mask at the Lyot plane needs to be as small as possible, not bigger than 2-3%. One-hour long exposures have confirmed the minimal impact of FPM dust particles and the achievable photon noise limited contrast goal.

References

[1] Roddier, F., "The Effects of Atmospheric Turbulence in Optical Astronomy", Prog. Optics, 9, 281-376 (1981).

[2] Marois, C., Doyon, R., Nadeau, D., Racine R., Walker G. A. H., "Effects of Quasi-Static Aberrations in Faint Companion Searches", EAS Publications Series, 8, 233-243 (2003).

[3] Macintosh, B. et al, "The Gemini Planet Imager", Proc. SPIE, 6272 (2006).

[4] Dohlen, Kjetil et al., "SPHERE: A planet finder instrument for the VLT", Proc. SPIE, 6269 (2006).

[5] Poyneer, L., Veran, J.-P., Dillon, D., Severson, S., Macintosh, B., "Wavefront control for the Gemini Planet Imager", Proc. SPIE, 6272 (2006).

[6] Soummer, R. et al., "Apodized Pupil Lyot Coronagraphs: Concepts and application to the Gemini Planet Imager", Proc. IAU #200, 367-373 (2006).

[7] Wallace, K. J., Bartos, R., Rao, S., Samuele, R., Schmidtlin, E., "A laboratory experiment for demonstrating post-coronagraph wavefront sensing and control for extreme adaptive optics", Proc. SPIE, 6272 (2006).

[8] Marois, C., Lafreniere, D., Doyon, R., Macintosh B., Nadeau, D., "Angular Differential Imaging: A Powerful High-Contrast Imaging Technique", ApJ, 641, 556-564 (2006).

[9] Racine, R., Walker, G. A. H., Nadeau D., Doyon, R., Marois, C., "Shades of Black: Searching for Brown Dwarfs and Giant Planets", PASP, 111, 587-594 (1999).

[10] Marois, C., Doyon, R., Racine, R., Nadeau, D., "Efficient Speckle Noise Attenuation in Faint Companion Imaging", PASP, 112, 91-96 (2000).

[11] Seager, S., hitney, B. A., Sasselov, D. D., "Photometric Light Curves and Polarization of Close-in Extrasolar Giant Planets", ApJ, 540, 504-520 (2000).

[12] Perrin, M. D., Sivaramakrishnan, A., Makidon, R. B., Oppenheimer, B. R., Graham, J. R., "The Structure of High Strehl Ratio Point-Spread Functions", ApJ, 596, 702-712 (2003).

[13] Marois, C., Phillion, D., Macintosh, B., "Exoplanet detection with simultaneous spectral differential imaging: effects of out-of-pupil-plane optical aberrations", Proc. SPIE, 6269 (2006).

[14] Krist, J. E., "PROPER: an optical propagation library for IDL", Proc. SPIE, 6675 (2007).

[15] Macintosh, B., Poyneer, L., Sivaramakrishnan, A., Marois, C., "Speckle lifetimes in high-contrast adaptive optics", Proc. SPIE, 5903, 170-177 (2005).

[16] Marois, C., Lafreniere, D., Macintosh, B., Doyon, R., "Accurate Astrometry and Photometry of Saturated and Coronagraphic Point Spread Functions", ApJ, 647, 612-619 (2006).

[17] Sivaramakrishnan, A., Oppenheimer, B. R., "Astrometry and Photometry with Coronagraphs", ApJ, 647, 620-629 (2006).

[18] Baraffe, I., Chabrier, G., Barman, T. S., Allard, F., Hauschildt, P. H., "Evolutionary models for cool brown dwarfs and extrasolar giant planets. The case of HD 209458", A&A, 402, 701-712 (2003).